Defence Research and Development Canada
Recherche et développement pour la défense Canada

DEFENCE R&D DÉFENSE

White-light burst generated during the filamentation of a Terawatt laser beam

F. Théberge
M. Châteauneuf
J. Dubois
P. Mathieu
DRDC Valcartier

Defence Research and Development Canada – Valcartier

Technical Report
DRDC Valcartier TR 2010-416
June 2011

Canada

White-light burst generated during the filamentation of a Terawatt laser beam

F. Théberge
M. Châteauneuf
J. Dubois
P. Mathieu
DRDC Valcartier

Defence Research and Development Canada – Valcartier

Technical Report
DRDC Valcartier TR 2010-416
June 2011

IMPORTANT INFORMATIVE STATEMENTS

Abstract

Defence Research & Development Canada—Valcartier (DRDC Valcartier) initiated many projects on femtosecond laser based counter-measure applications. One of the main properties of high peak power femtosecond laser pulses is their transformation into a white-light supercontinuum, which can be exploited for dazzle (and possibly damage) counter-measure purposes. Contrary to normal dazzle generated using a narrow-spectrum laser source, the white-light surpercontinuum from femtosecond laser pulses spans continuously from the ultraviolet up to the infrared. Such broadband white-light lasers are virtually impossible to block because they do not rely on a single wavelength to achieve the effect. This report presents the characterization of the white-light laser burst produced during the propagation in air of a femtosecond-Terawatt laser. The supercontinuum was generated from 200 nm in the ultraviolet up to 13.6 μm in the far infrared, which led to the first worldwide demonstration of such a broadband laser source.

Résumé

Recherche et développement pour la défense Canada—Valcartier (RDDC Valcartier) a entrepris plusieurs projets sur les sources lasers femtosecondes pour des applications de contre-mesures. L'une des principales propriétés des impulsions laser femtoseconde de haute puissance est leur transformation en une impulsion de lumière blanche qui pourrait être utilisée comme contre-mesure pour éblouir (et possiblement endommager) les détecteurs optiques. Contrairement aux contre-mesures laser basées sur des sources à spectres étroits, l'impulsion de lumière blanche générée par le laser femtoseconde comporte un spectre très large pouvant s'étendre de l'ultraviolet jusqu'à l'infrarouge. Un tel laser blanc est virtuellement impossible à contrer, car il n'est pas basé sur une seule longueur d'onde pour générer l'effet désiré. Ce rapport présente la caractérisation de l'impulsion laser blanche produite durant la propagation d'un laser femtoseconde-térawatt dans l'air. Le supercontinuum du laser blanc s'étend de 200 nm dans l'ultraviolet jusqu'à 13,6 μm dans l'infrarouge lointain, ce qui correspond à la première démonstration mondiale d'une telle source laser à très large spectre.

This page intentionally left blank.

Executive summary

White-light burst generated during the filamentation of a Terawatt laser beam

F. Théberge; M. Châteauneuf, J. Dubois; P. Mathieu; DRDC Valcartier TR 2010-416; Defence R&D Canada – Valcartier; June 2011.

Introduction: Over the recent years, Defence Research & Development Canada — Valcartier (DRDC Valcartier) has developed a new niche of expertise in ultra-intense laser-pulse technologies. The investment in a unique world-class portable terawatt femtosecond laser has already made DRDC a major player in the limited scientific community of ultra-intense short-pulse lasers. Moreover, the significance of the research projects combined with the expertise at DRDC Valcartier on that subject has stimulated partnerships with Canadian universities, and international collaborations with other research organizations.

Results: The propagation of femtosecond-terawatt lasers in the atmosphere demonstrated numerous potential applications for the defence such as the remote generation of white-light laser burst, the creation of a long conductive plasma channel and the guiding of microwaves. This report focusses on one of the main properties of femtosecond-terawatt laser, which is its transformation into a white-light burst that can be exploited for dazzling and possibly damaging optical devices for counter-measure applications.

Significance: Contrary to typical dazzling generated using a narrow spectrum laser, the white-light laser burst spans continuously from the ultraviolet to the infrared. Such broadband white-light laser is virtually impossible to block in an optical system because it does not rely on a single wavelength. The spectral extension of the femtosecond-terawatt laser propagating in air was so broad that the generated white-light laser burst could overpass the absorption band of the air and produce remote infrared sources in the 3-5 μm and 8-12 μm transmission windows of the atmosphere. The peak intensities of the generated infrared pulse inside each filament were around 50 MW/cm^2 and 50 kW/cm^2 in the mid-infrared and far-infrared spectral regions, respectively. The spectrum of the white-light laser burst was generated and characterized from 200 nm in the ultraviolet up to 13.6 μm in the far-infrared, which led to the first worldwide demonstration of such broadband laser source.

Future plans: Now that the white-light laser burst is characterized, the impact of turbulent atmosphere and the propagation of femtosecond-terawatt lasers under different atmospheric conditions also need to be studied. The results presented in this report also suggest that the spectral intensity of the infrared supercontinuum could be strongly enhanced by mixing two delayed pump pulses or by mixing a pump pulse with another laser pulse in the visible range. A better understanding of the nonlinear propagation of these intense laser pulses will allow the optimization of the white-light burst at long range in the atmosphere. The better understanding will also maintain Canada's lead in the experimental work on the propagation of high peak power lasers in the atmosphere.

Sommaire

White-light burst generated during the filamentation of a Terawatt laser beam:

F. Théberge; M. Châteauneuf, J. Dubois; P. Mathieu; DRDC Valcartier TR 2010-416; R & D pour la défense Canada – Valcartier; June 2011.

Introduction: Au cours des dernières années, Recherche et développement pour la défense Canada — Valcartier (RDDC Valcartier) a développé un nouveau créneau d'expertise sur les impulsions laser ultra-intenses. L'investissement récent dans un laser femtoseconde-térawatt portable de classe mondiale a permis à RDDC de se positionner comme acteur majeur dans la communauté scientifique des technologies laser femtoseconde ultra-intenses. De plus, l'importance des projets de recherche, combinée à l'expertise de RDDC Valcartier dans ce domaine a rendu possible des partenariats avec des universités canadiennes et des collaborations internationales avec d'autres groupes de recherche.

Résultats: La propagation d'impulsions laser femtoseconde-térawatt dans l'atmosphère a démontré plusieurs applications potentielles pour la défense, comme l'éblouissement par la lumière blanche, la formation de longs canaux de plasma conducteurs et le guidage de micro-ondes. Ce rapport couvre une des principales propriétés des lasers femtoseconde-térawatt, qui est leur transformation en une impulsion laser blanche pouvant être exploitée en contre-mesure pour éblouir et possiblement endommager les systèmes optiques.

Importance: Contrairement aux systèmes de brouillage laser basés sur des sources à spectre étroit, les impulsions laser blanches possèdent un spectre pouvant s'étendre de l'ultraviolet jusqu'à l'infrarouge. Un tel laser blanc est virtuellement impossible à bloquer, car il n'est pas basé sur une seule longueur d'onde pour générer l'effet désiré. Le contenu spectral de ces lasers blancs est tellement large qu'il peut être généré au-delà des bandes d'absorption de l'atmosphère et produire à longue distance une source laser infrarouge dans les fenêtres de transmission de 3-5 μm et 8-12 μm. L'intensité crête de ces impulsions infrarouges dans les filaments produits par le laser femtoseconde-térawatt est d'environ 50 MW/cm^2 et 50 kW/cm^2 dans l'infrarouge moyen et l'infrarouge lointain, respectivement. Le spectre de l'impulsion laser blanche a été caractérisé à partir de 200 nm dans l'ultraviolet jusqu'à 13,6 μm dans l'infrarouge lointain, ce qui correspond à la première démonstration mondiale d'une telle source laser à très large spectre.

Perspectives: Maintenant que l'impulsion laser blanche a été caractérisée, l'impact des turbulences dans l'atmosphère et la propagation du laser femtoseconde-térawatt dans différentes conditions météorologiques nécessitent d'être étudiés également. Les résultats présentés dans ce rapport indiquent également que l'intensité spectrale du supercontinuum infrarouge pourrait être grandement accrue en superposant deux impulsions laser décalées temporellement ou en superposant deux impulsions laser de longueur d'onde différente. Une meilleure compréhension de la propagation nonlinéaire du laser femtoseconde-térawatt nous permettra d'optimiser la génération d'impulsion laser blanche à longue distance dans l'atmosphère. Il permettra également de maintenir le leadership du Canada dans les travaux expérimentaux sur la propagation d'impulsions laser ultra-brèves et intenses dans l'atmosphère.

Table of contents

List of figures

List of tables

Acknowledgements

The authors wish to acknowledge Mr. Vincent Ross from AEREX Avionics for his precise simulations of the index of refraction of air over a very large spectral range. These valuable simulations have been fruitful for the understanding of the broadband IR pulse generated during the filamentation of femtosecond-terawatt laser in the atmosphere.

The authors would also like to acknowledge the very valuable technical support from Ms. Michèle Cardinal and Mr. Marcellin Jean from the Electro-Optical Warfare Section for the preparation of the experimental setup, and the installation of the *Terawatt & Terahertz Laboratory* (*T&T Lab)*.

1 Introduction

During the last decade, propagation of powerful laser pulses over long distances in air has attracted a lot of interest due to particular optical processes occurring during its transmission in the atmosphere. When a powerful and ultrashort laser pulse propagates in air, the propagation behaviour of the laser beam is completely different to that of continuous wave or long-pulse lasers. For TW and fs laser pulses, there are numerous nonlinear optical effects that are involved during their propagation such as the Kerr self-focusing, the self-diffraction of plasma, and the spectral broadening. From the dynamic interactions of these nonlinear processes that result in novel laser properties such as the self-collimated beam over long distance [1], the self-stabilization of the laser [2-4], and the remote generation of white-light burst.

More than being of high scientific interest, the filamentation of ultrashort laser pulses represents a promising application for Defence - over recent years, DRDC Valcartier has been involved in research projects on intense ultrashort laser pulses. During their propagation in the atmosphere, these fs laser pulses can induce the ionization of the air and create a conductive plasma channel along its path. Such plasma channel can be used to guide other energy sources like microwave [5] and high voltage [6] for CMs against IEDs, rockets or other similar threats. The use of filamenting laser pulses allows to scan a large area or quickly aim the laser in the direction of the threat. Moreover, a filamentating laser pulse would modify its spectral distribution during the propagation and would evolve into a continuous broadband (white-light) laser pulse, which can be used for dazzling of optical devices, independently of the spectral range used by the threat. The broadband beam of light resulting from filamentation consists in an intense white center (the white-light supercontinuum) surrounded by a CE. This CE is due to self-phase modulation from the plasma produced in the filament.
The white-light supercontinuum generated by these filaments in air can be exploited for dazzling (and possibly damaging) CM purposes. Contrary to normal dazzle generated using a narrow spectrum laser source, the white-light surpercontinuum, due to its spectrum extending from the UV to the IR, is virtually impossible to block because it does not rely on a single wavelength to achieve the effect. Furthermore, white-light dazzling is independent of the spectral range used by the optical detector of the threat. Moreover, as illustrated in Figure 1, the remote generation of a white-light burst from the filamenting pulses could also be used as a false target in order to mislead laser-guided threats.

This report presents the spectral characterization of the white-light laser pulse generated during the filamentation in the air of a fs-TW laser pulse. The obtained results show that the spectrum of the filamenting pulse could span from the UV up to the IR. The spectral extension was so broad that the generated white-light laser pulse could overpass the absorption band of air and produce remote IR sources in the 3-5 μm and 8-12 μm transmission windows of the atmosphere.

In order to better understand the experiment and the results presented in this report, more details on the physical process for the laser spectral broadening is discussed in the next section. Section 3 presents the spectrometer built at DRDC-Valcartier that allows us to measure for the first time the white-light supercontinuum from the UV up to the FIR, and over 12 orders of magnitude in

dynamic range. Finally Section 4 shows the measurements of supercontinuum from a filamenting laser pulse.

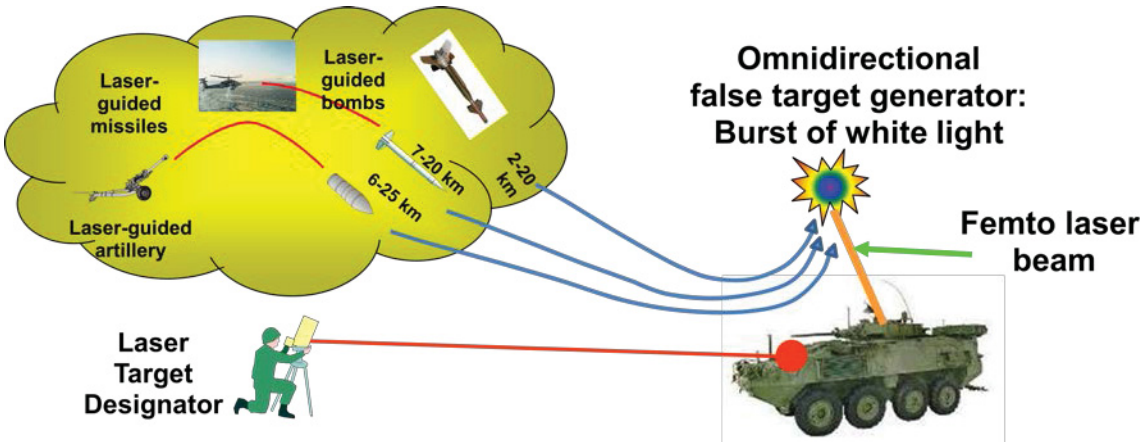

Figure 1. Illustration of false target generation from a filamenting femtosecond laser beam.

2 Physics of filamentation

By definition, the filamentation is a nonlinear phenomenon whereby the pulsed laser beam propagates with a contracted diameter over a distance much longer than the Rayleigh length. Filamentation was first observed in 1964 by Hercher as he studied the optical damage in solids [7]. He found that by focusing into a solid a Q-switched laser beam of more than a few megawatts, one obtained long threads of damage spots. In the 1970s, many investigations on the filamentation phenomenon were carried out with ns and ps laser pulses [8, 9]. However, due to the limitations in laser power at that time, the filamentation studies were limited to condensed matters having a self-focusing power threshold at the megawatt (MW) level. Owing to the development of the CPA technique [10, 11], it has been possible to achieve fs laser pulses with TW level peak power. Nonlinear phenomena during propagation of such intense ultrashort laser pulses become much more pronounced than for longer pulses and could be observed in the air.

2.1 Review of laser filamentation

The filamentation in air cannot be observed below a peak power threshold, Pcr, which is the critical power for self-focusing. In air, this Pcr is about few GW. If the peak power of the laser pulse is below this threshold, this laser pulse propagates linearly like common laser pulses. However, if the peak power of the laser is above this threshold, the laser pulse collapses on itself and generates an optical filament. Here, the term "filamentation" denotes an extended light string whereas the beam contracts and maintains a narrow diameter over a distance much longer than the Rayleigh range of a focused beam. By definition, the Rayleigh length of a laser beam corresponds to the axial distance within which the beam radius lies within a factor $\sqrt{2}$ of its minimum value.

Filamentation of optical laser pulses is a universal phenomenon that occurs during the propagation of a powerful ultrashort laser pulse in any optical medium. The filamentation is governed by the dynamic interplay between the optical Kerr effect due to the intensity-dependent refractive index and defocusing from a low-density plasma induced by the ionization of the optical medium (for recent reviews, see Ref. [12] and Ref. [13]). The defocusing effect of the generated plasma balances the self-focusing effect and leads to a limited peak intensity of about 5×10^{13} W/cm^2 during the laser pulse propagation in air [14, 15]. This is known as intensity clamping. The onset of the filamentation process can be manipulated by controlling the initial beam diameter, focusing and pulse duration [12, 16].

In order to visualize the self-focusing and the filamentation of a laser pulse, let's assume an intense ultrashort laser pulse having both a Gaussian temporal profile and a Gaussian spatial profile. Because of the high peak power of such laser pulse, the effective index of refraction (n) of the optical medium would depends on the laser intensity, and it is given by:

$$n(r,t) = n_0 + n_2 * I(r,t) \quad (1)$$

where n_0 is the linear index of refraction (in air, $n_0 \cong 1.0003$ in the visible range), n_2 is the nonlinear index of refraction and $I(r,t)$ is the instantaneous laser intensity and depends on the radial (r) and temporal (t) coordinates. It should be noted that the value of n_2 in air is approximately $10^{-19}\ cm^2/W$, and in order to significantly affect the index of refraction, a laser with very high peak intensity is needed. At the moment, the relative contribution of higher order nonlinear Kerr terms (n_4*I^4, n_6*I^6, n_8*I^8, etc.) to the filamentation of intense laser pulses have not been clarified yet, and their values were not measured precisely. Therefore, we will neglect these terms. With a powerful laser having a Gaussian profile, the laser intensity is higher at the center of the laser pulse and lower at the outer zone. Thus, the effective index of refraction is more important in the center (and this center part of the laser pulse propagates more slowly due to the higher index of refraction) than the outer edges. As a result, a curvature of the wavefront is induced, which is similar to that induced by a focusing lens. This type of phenomenon is called self-focusing. As shown in Figure 2, when the laser intensity is sufficiently high, the wavefront will continue on curving forward as the laser pulse propagates further.

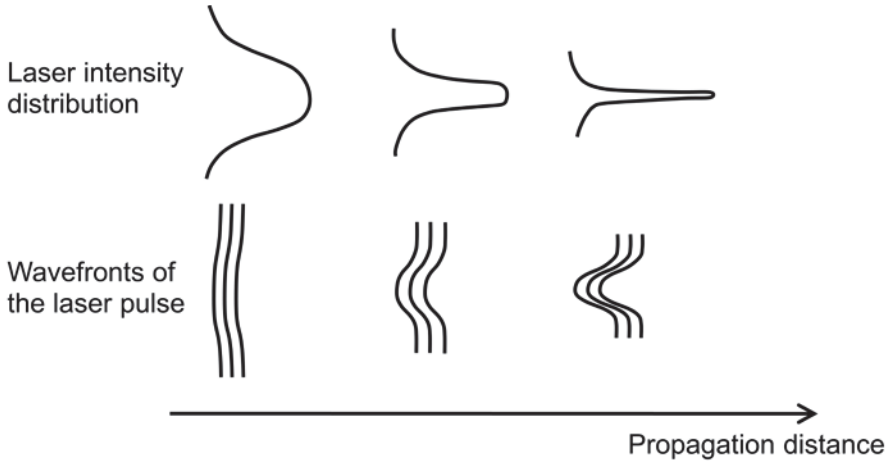

Figure 2. *Schematic illustration of the self-focusing of a femtosecond laser pulse in an optical medium. The laser pulse has an initial Gaussian intensity distribution across the transverse plane.*

According to the slice-by-slice self-focusing scenario [17] or the dynamic spatial replenishment model [18], each section of the laser pulse has a different laser intensity and tends to self-focus at different distances. Each slice contains a specific power, and the thickness of each slice is equal to $c * \tau$, where c is the speed of light and τ is an optical cycle of the electromagnetic wave. This is because the intensity of an electromagnetic wave is represented by the Poynting vector averaged over at least one optical cycle. As shown in Figure 3, the series of self-foci originating from each slice (having different power P1, P2, and P3) gives rise to the perception of a filament. The slices with peak power below the critical power P_{cr} simply diffract out linearly.

The self-focusing distance (z_f) for each slice having a peak power above P_{cr} is determined by [8]:

$$z_f = \frac{0.367ka^2}{\left\{\left[\left(\frac{P}{P_{cr}}\right)^{1/2} - 0.852\right]^2 - 0.0219\right\}^{1/2}} \tag{2}$$

where k is the wavevector of the laser pulse, a is the beam radius defined at 1/e level of the intensity, and P is the initial power of the slice. Thus, a laser beam having a larger radius tends to self-focus at longer distance. Figure 4 illustrates more precisely the power distribution inside the laser pulse, and it can be seen that the self-focusing distance increases quickly as the instantaneous power decreases along the temporal profile. For a laser pulse having a pulse duration of 50 fs at full width at half maximum (FWHM), a beam radius of 5 mm and an initial peak power of $2P_{cr}$, the value of z_f for each laser slice extends from 140 m up to the km range. However, according to Eq.(2), by tripling the diameter of the laser beam (a=1.5 cm), the self-focusing, and thus the filamentation, starts at 1.2-1.3 km away from the laser source.

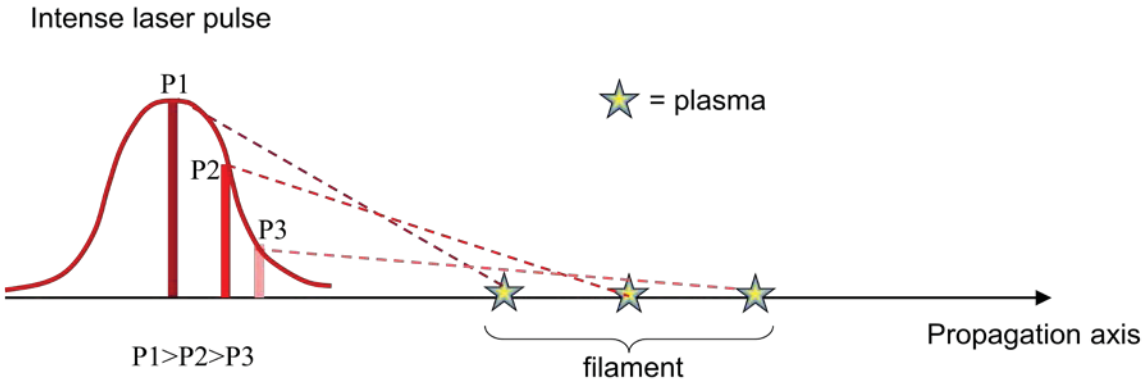

Figure 3. Illustration of slice-by-slice self-focusing of a laser pulse.

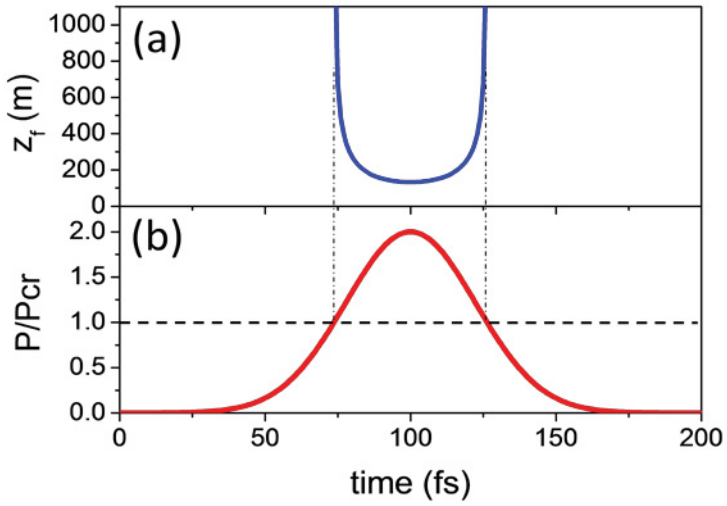

Figure 4. (a) Self-focusing distance of different "slice" of a 50-fs laser pulse presented in (b). The dash line in (b) indicates the threshold where the instantaneous power of the laser pulse is above or below the critical power for self-focusing (P_{cr}).

During the self-focusing, the intensity of the laser pulse becomes higher and higher. As a result, the on-axis intensity becomes sufficiently high to ionize the air through the multiphoton absorption and to generate a weak plasma. The emergence of the plasma results in a decrease of the effective index of refraction on the propagation axis, and Eq. (1) should be rewritten according to:

$$n(r,t) = n_0 + n_2 * I(r,t) - \omega_p/2\omega_0 \tag{3}$$

where ω_p is the plasma frequency and ω_0 is the central frequency of the laser pulse. In air, the plasma density (N_e) in the filament generated by an optical laser pulse has been measured to be of the order of 10^{16} electrons/cm^3 and the corresponding plasma frequency is $\omega_p = \sqrt{4\pi e^2 N_e/m_e} = 5.6 \times 10^{12}$ Hz. Such plasma frequency is much smaller than the frequency of a laser ($\omega_0 \sim 5 \times 10^{14}$ Hz), and thus the light is easily transmitted through such plasma. However, the plasma generation depends nonlinearly of the laser intensity. According to the ionization potential of both oxygen and nitrogen (major constituents in air), most of the plasma generated in air originates from these two gases, and the plasma density depends mostly as the power 9 of the laser intensity, i.e. $N_e \propto I^9$. The lifetime of this plasma is of the order of few nanoseconds, thus one million times longer than a fs laser pulse timescale. Therefore, the recombination and diffusion of the electrons can be neglected during the interactions of the laser pulse. The plasma generation is a highly nonlinear intensity-dependent process; consequently, most of the plasma is generated at the center of the laser pulse where the laser intensity is the highest. However, due to the long lifetime of the plasma relative to the laser pulse duration, the back part of the laser pulse "feels" the plasma generated by the central part. Conversely, the front part of the laser precedes the central part, and thus the front part of the laser pulse is not affected by the plasma generated by this central part. Thus the effective plasma density "seen" by each part of the laser pulse at the time *t* is given by

$$N_e(r,t) = N_0 w \int_{-\infty}^{t} I^9(r,t')\, dt' \tag{4}$$

where N_0 is the density of the neutral air and w is the effective ionization rate of air (mainly from oxygen and nitrogen). Finally the effective index of refraction would be expressed as follows [12]:

$$n(r,t) = n_0 + n_2 I(r,t) - \frac{4\pi e^2 \left[N_0 w \int_{-\infty}^{t} I^9(r,t')dt' \right]}{2m_e \omega_0^2} \tag{5}$$

The filamentation process is always accompanied by a spectral broadening of the laser pulse, which is due to the temporal phase modulation of the effective index of refraction. Such an effect is presented in Figure 5 where a digital picture of the filamenting pulse has been taken on a white diffuser screen. The laser beam was initially convergent by using a telescope with a effective focal length of 100m. In this condition an 20m long filament is observed starting at 70m from the telescope. The initial fs laser pulse was centered at 800 nm (near IR) and its spectral width broadened during the filamentation to cover the visible range completely. It is interesting to note that the shorter wavelengths are observed at larger angles from the propagation axis: such a spectral distribution corresponds to the CE.

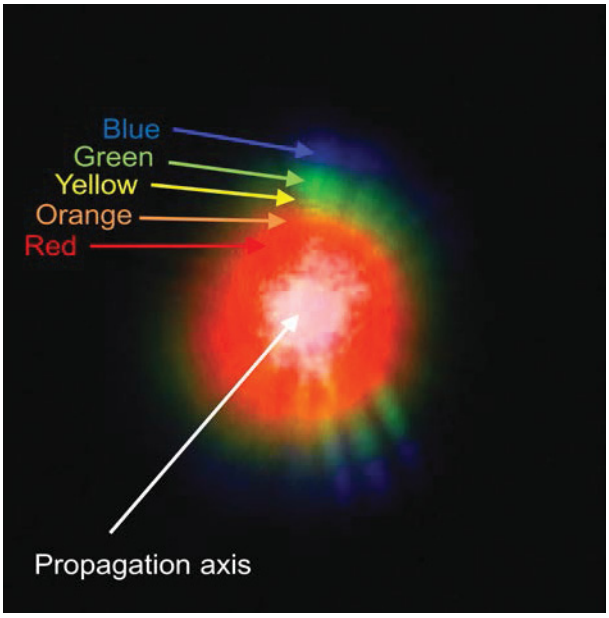

Figure 5. White-light beam profile generated 100 m away from the laser source. The parameters of the laser pulses were 190 mJ/pulse, 500 fs of pulse duration, beam diameter was 8 cm at FWHM.

During filamentation, the temporal shape of the laser pulse is strongly reorganized [12, 13]. The temporal variation of the laser intensity induces a temporal variation in the effective index of

refraction as pointed out in Eq 5. Such modulation of the effective index of refraction induces an inflection of the laser pulse's phase (ϕ_{NL}), which involves the appearance of new frequencies in the laser spectrum. This effect is termed as SPM and the corresponding frequency shift ($\Delta\omega$) is given by:

$$\begin{aligned}\Delta\omega &= \frac{\partial \phi_{NL}}{\partial t} \\ &= \frac{\partial}{\partial t}\left(-\frac{\omega_0 \Delta n(t)}{c} z\right) \\ &= -\frac{\omega_0 z}{c}\frac{\partial[\Delta n(t)]}{\partial t}\end{aligned} . \tag{6}$$

As shown in the last term of equation 6, the new frequencies generated depend on the slope of the variation of the index of refraction (Δn), and the propagation distance z in the optical medium [12]. When the laser pulse self-focuses and creates a filament, the front part of the laser pulse always sees a neutral medium; it is the central part of the laser pulse that mainly generates the plasma and it is the back of the laser pulse that mostly "sees" the plasma. By introducing Eq. (5) into Eq. (6), the frequency shift in the front part of the laser pulse can be noted as:

$$\Delta\omega = -\frac{\omega_0 z}{c} n_2 \frac{\partial I(front\ \ part)}{\partial t} . \tag{7}$$

Thus the SPM at the front part of the laser pulse induces a negative frequency shift ($\Delta\omega < 0$) because the temporal slope of the laser intensity is positive at the front part. Such a frequency shift is commonly named a red-shift.

Conversely, the back part of the laser pulse sees both the neutral medium and the plasma because the optical medium is only partially ionized by the filamenting laser pulse. By introducing Eq. (5) into Eq.(6) again, the frequency shift in the back part of the laser pulse is given by:

$$\Delta\omega = -\frac{\omega_0 z}{c} n_2 \frac{\partial I(back\ \ part)}{\partial t} + \frac{2\pi e^2 z}{c m_e \omega_0}\frac{\partial}{\partial t}\left[N_0 w \int_{-\infty}^{t} I^9(t')dt'\right] . \tag{8}$$

The last term of Eq. (8) contains a temporal integration followed by a temporal derivation. The two processes cancel each other out because no singularities can occur inside the temporal distribution of the laser intensity. Therefore, the Eq. (8) should be rewritten as follows:

$$\Delta\omega = -\frac{\omega_0 z}{c} n_2 \frac{\partial I(back\ \ part)}{\partial t} + \frac{2\pi e^2 z}{c m_e \omega_0} N_0 w I^9(t) . \tag{9}$$

The first term in Eq. (9) gives a positive frequency shift due to the negative temporal slope at the back of the laser pulse. The second term corresponds to the plasma contribution, which also predicts a positive frequency shift. In the real case, the presence of the plasma reshapes the back part of the laser pulse. The intensity distribution of the pulse becomes steeper, which gives rise to a more important blue-shift relative to the red-shift observed at the front part of the laser pulse. It is important to note that both the red-shift and the blue-shift are linearly proportional to the filament length (z), and thus a longer filament would induce a larger frequency shift.

The rainbow-like CE in Figure 5 is due to the SPM in the radial direction of the laser pulses [12]. The above discussion on the spectral broadening considered only the part of the wavefront centered on the propagation axis (named z-axis). For a filamenting laser pulse, the wavefront is curved and the general expression of the wave vector $\vec{k}$ contains both a longitudinal k_z component and a transverse part k_r according to:

$$\vec{k} = k_z\hat{z} + k_r\hat{r} = k_{z0}\hat{z} + \Delta k_z\hat{z} + k_{r0}\hat{r} + \Delta k_r\hat{r} \quad (10)$$

where $\hat{z}$ and $\hat{r}$ are the unit vectors parallel and orthogonal to the propagation direction z; k_{z0} and k_{r0} are the initial wave vectors components along $\hat{z}$ and $\hat{r}$, respectively. In the off-axis direction ($\hat{r}$), the electron density is maximal on the propagation axis and decreases in the radial direction. Such gradient of the electron density will give rise to a larger $\vec{k}$ (blue-shift) at larger divergence angle because

$$\Delta k_r = \left|\frac{\partial \phi_{nl}}{\partial r}\right| \propto \left|\frac{\partial N_e}{\partial r}\right| \quad (11)$$

This radial electron density gradient varies continuously from zero to a maximum. The divergence of the general wave-vector is larger when the electron density gradient is larger. Also, a larger divergence (larger Δk_r) due to the plasma implies a larger wave vector $\vec{k}$ because $|\vec{k}| \cong \sqrt{k_0^2 + (\Delta k_r)^2}$, and thus implies a larger spectral shift. Consequently, as shown in Figure 5, the larger blue-shift of the laser pulse is observed at a larger divergence angle. For the red-shift spectral components, which are mainly generated on the front part of the laser pulse (where there is no plasma), the theory based on the SPM predicts that these spectral components remain on the propagation axis where we can observe a white-light central spot.

2.2 Multiple filamentation

In real experimental conditions, the laser peak power is often much higher than the critical power for self-focusing and results in the creation of multiple filaments. The explanation for the formation of multiple filaments is schematically shown in Figure 6a. For a laser beam having multiple maxima in its intensity distribution, each maximum induces a higher index of refraction

due to the nonlinear Kerr effect. Then each maximum in the laser intensity distribution would propagate more slowly (due to the higher index of refraction) than their surrounding parts. As a result, the wavefront of each maximum curves on itself and creates its own white-light filament as shown in Figure 6b. The wavefront curvature for each intensity maximum varies depending on its initial peak intensity and the initial radius of the "hot" spot. Therefore, each hot spot in the beam profile might self-focus (see Eq. 2) at different distance. These hot spots in the initial beam profile can be due either from inherent imperfections of the laser beam profile or due to external perturbation such as turbulence in air or the passage through a non-uniform optical component, etc. These distortions lead to more than one maximum intensity zone across the beam profile. This eventually induced multiple filaments along the propagation path of the fs-TW laser beam.

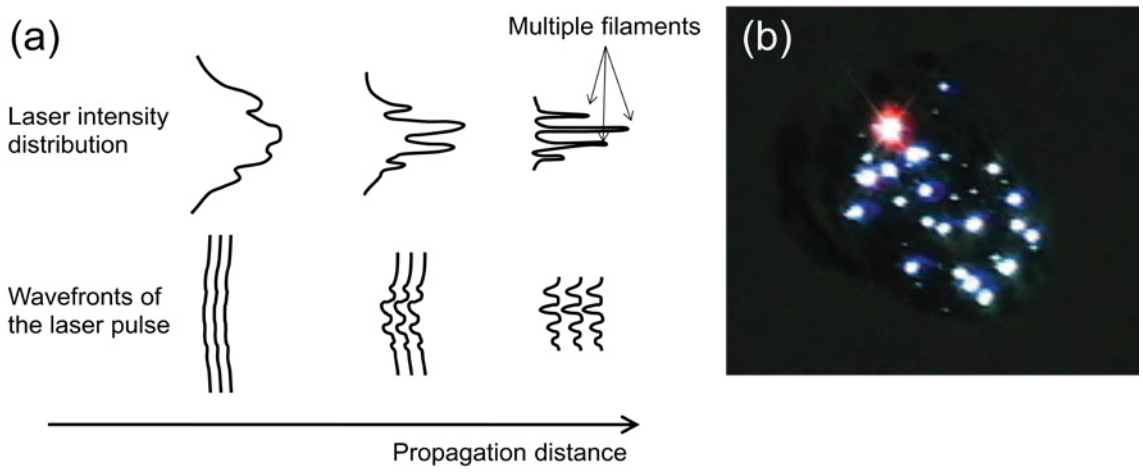

Figure 6. (a) Schematic illustration of multiple filamentation of a femtosecond laser pulse in an optical medium. (b) Picture of multiple filaments taken by a digital camera.

3 Measurement of supercontinuum

Filamentation can be used in a wide range of applications ranging from the remote sensing in the atmosphere using the backward-emitted fluorescence from the plasma [19], the guiding of electric discharge through the plasma channels [20], the guiding of microwaves [5, 21], and generation of white-light laser burst for dazzling applications. As described in Section 2, the physical mechanism of the filamentation is complex in the sense that there are many nonlinear processes taking place simultaneously. Although the understanding of optical filamentation is now considered to have reached a high level of maturity, there are still a large number of interacting effects occurring in the filament that have not yet been thoroughly studied. So far, only a few research groups have analyzed the propagation of fs-TW laser pulses in the atmosphere and for the CM applications, there is a need to characterize its spectral transformation during the filamentation. Until now, the spectral distribution of the supercontinuum generated in air has been measured from the UV [22] up to 4 μm by the pioneering works of Kasparian *et al.* [23]. However, for this last result dating from year 2000, the measured IR extension was recorded only at the center of the white-light laser beam and was limited by the weak sensitivity of the detectors used.

This report, presents the characterization of ultra-broadband white-light laser and CE during the filamentation in air of fs-TW laser pulses produced by the *T&T* lab. The supercontinuum produced by this laser spans from 200 nm up to 13,6 μm and completely covers the optical transmission window of the atmosphere. This section of this report briefly describes the T&T laser used to produce the optical filament and the spectrometer built to characterize the supercontinuum over a broad spectral range and over a large dynamic range.

3.1 Terawatt &Terahertz Laboratory

The *T&T* portable laser facility used for these experiments is a 5 TW Ti:Sapphire laser system delivering 225 mJ per pulse with a pulse duration of 42 fs. The central wavelength is 805 nm and the pulse repetition rate is 10 Hz. The compact laser system sits on a 1.25 m by 2.5 m optical table. The laser system was integrated into a standard sea container into which a modular clean room of class 100,000 was inserted. The clean room occupies about half of the container; the remaining part being used as a control room. A schematic of the interior of the container and photographs of the finalized laboratory are shown in Figures 7 and 8, respectively.

The air pressure in the clean room is slightly higher than the adjacent room and the temperature is kept to 20° ±1° Celsius. These conditions can be maintained with an exterior temperature ranging from -30° to 30° Celsius and with an opening in the clean room of 15 cm in diameter to allow the propagation of the laser beam to the exterior with minimum distortion. The optical table onto which the laser system is installed is mounted on two sets of pneumatic isolators. The first set is used when the container is stationed and the laser is in operation; while the second set, more rigid, is used during transportation. A breadboard is fixed in a rack over the laser system. This second layer is used to mount small optical setups to characterize the laser beam or to shape it to match the experiments requirements. The rack is fixed to the optical table such that movements and vibrations of the laser and the breadboard are coupled together. There are four 15-cm openings to

propagate the beam outside the portable laboratory: two through the rear door for propagation at the output of the compressor or from the upper breadboard; one through the ceiling; and one through the wall at the height of the breadboard. In order to maintain the clean room conditions, only one aperture is opened at a time. The control room is filled with the air conditioning unit, the power supplies, and chillers for the laser systems as well as the control rack. The user is able to fully control the laser either from the clean room, the control room, or from the exterior of the container via an Ethernet link. The control room also acts as an airlock for the clean room.

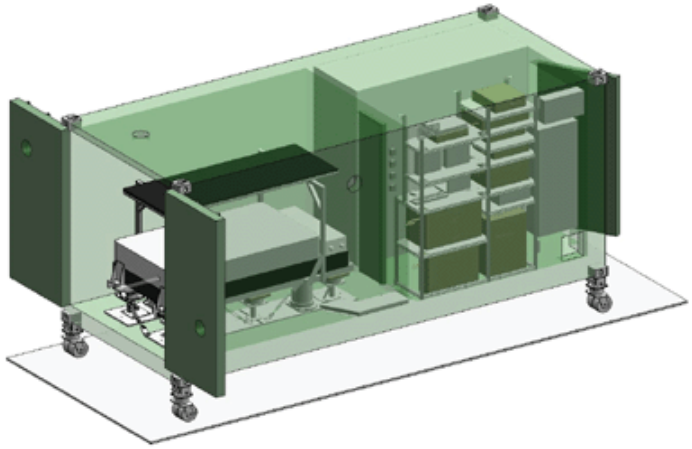

Figure 7. Schematic of the interior of the T&T container (the clean room with the laser system are shown on the left-hand side and the control room is at the right-hand side of this schema).

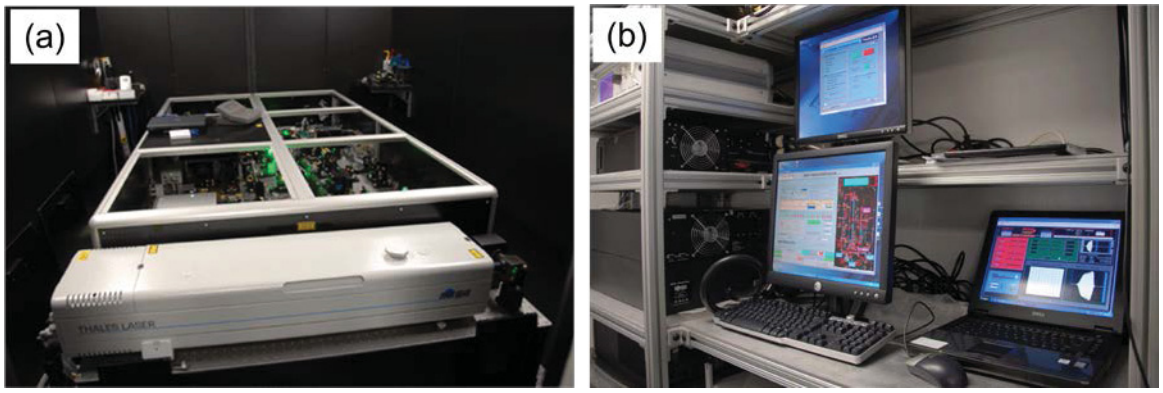

Figure 8. *Pictures of (a) the TW laser inside the container and (b) diagnostic rack and monitoring computers in the control room.*

3.2 Broadband Spectrometer

For the experiments reported in this report, the diameter of the beam at the output of the optical compressor was 2.5 cm at FWHM, and the laser beam was focused in air and by a 4 m focal length concave mirror. Energies between 35 mJ up to 70 mJ were used to generate filaments starting around 2.5 m after the concave mirror and ending near its geometrical focus. The angularly resolved spectrum of the generated supercontinuum in air was measured with five different spectrometers (one used at time) set on a motorized rotation stage (Figure 9). The main rotation axis in Figure 9 was centered on the filaments, and the spectrometers were located at the end of this 3 m long rotation arm in order to measure the spectral distribution of the CE as a function of the divergence angle.

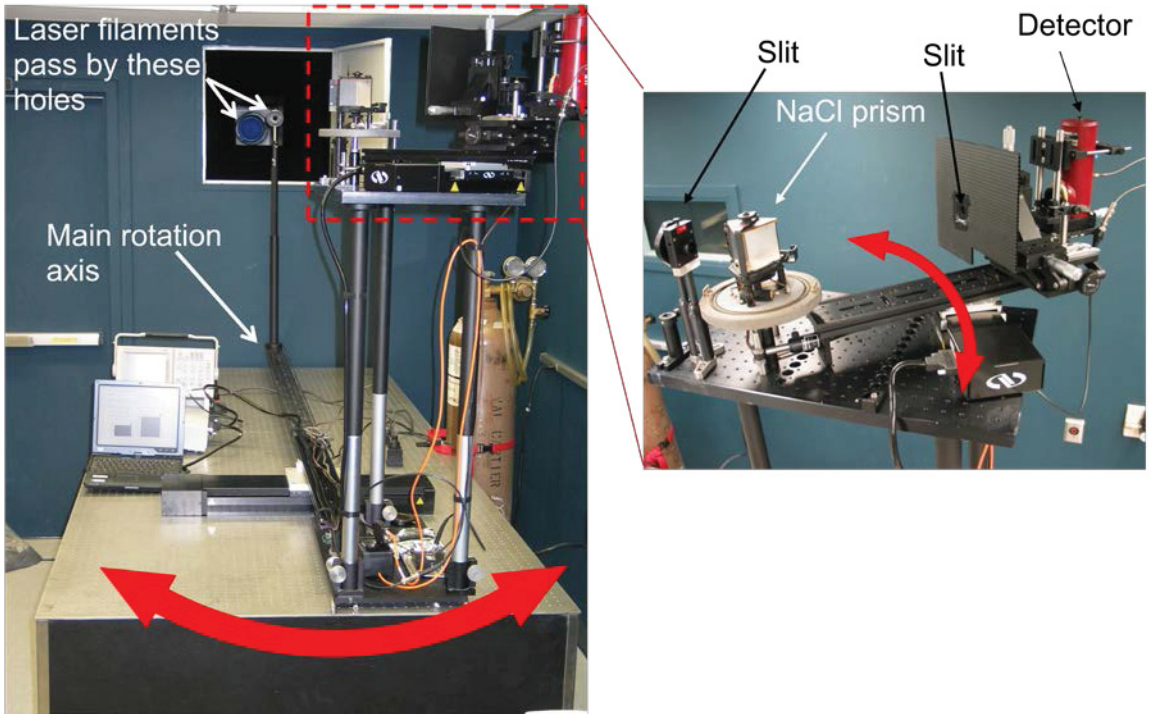

Figure 9. Pictures of the broadband spectrometer used to characterize the supercontinuum.

For the infrared signal above 1 μm, we could not use a standard spectrometer based on dispersive grating, because the diffracted angle (θ_m) is given by:

$$sin(\theta_m) = m\lambda/d - sin(\theta_i) \quad (12)$$

where m is a integer corresponding to the diffraction order, λ is the wavelength, d is the grating groove period, and θ_i is the incident angle of the beam. As a result, for a broadband spectrum (which can span over many octaves), the used of a grating spectrometer superposes different diffraction orders at the same position on the detector if the product $m\lambda$ is the same (Figure 10a).

For example, the second order of diffraction (m=2) from the signal at 400 nm (blue light) is diffracted at the same angle as the first order of diffraction (m=1) from the signal at 800 nm (red light). Thus, it becomes impossible to distinguish the 400 nm from the 800 nm signals. The same problem occurs at longer wavelengths in the infrared. For this reason, it was necessary to build a monochromator based on the dispersion of a NaCl prism. In the case of a prism, there is a single dispersed beam (see Figure 10b), and each wavelength is refracted at a different angle.

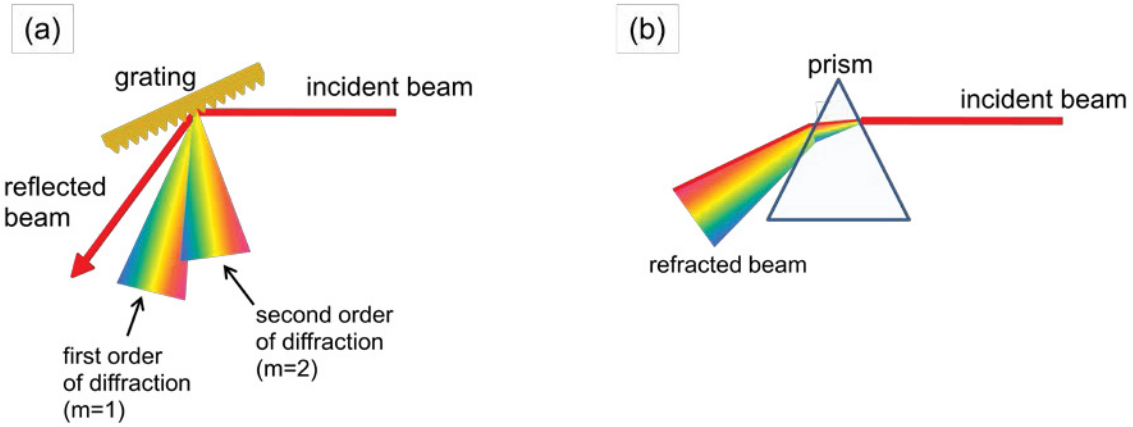

Figure 10. *Schematic of the dispersion from (a) a grating and (b) a prism (in (a), the blue light of the second order of diffraction is superposed onto the red light of the first order of diffraction).*

Two detectors *having a different spectral response* were used with the monochromator: a liquid-nitrogen-cooled MCT, and a PbSe photodiode. The calibration of this monochromator is shown in Figure 11, and has been done using the CE itself and a series of IR bandpass filters. The angular resolution of this system was 0.1 mrad, and the spectral resolutions for the different spectrometers used are listed in Table 1. The complete spectral distribution was reconstructed by overlapping the common spectral ranges of each spectrometer/monochromator. The reconstructed spectrum covered a dynamic range of 12 orders of magnitude for the intensity and six octaves for the spectral range starting at the wavelength of 200 nm up to 13.6 μm.

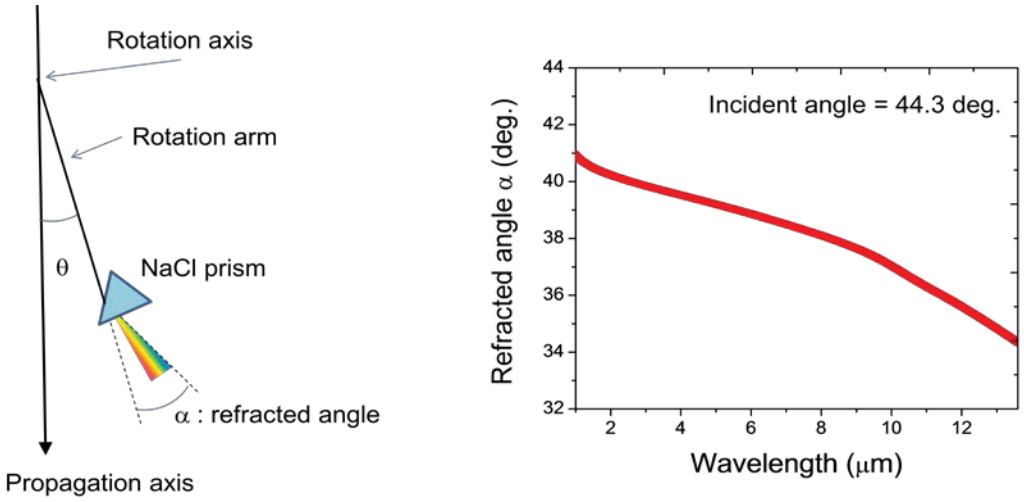

Figure 11. *Calibration of the prism monochromator (the graph presents the refracted angle as a function of the wavelength).*

Table 1. Spectral ranges and resolutions of the spectrometers used for the measurements of the broadband white-light laser.

Spectrometers	**Spectral range**	**Resolution**
QE65000 from *OceanOptics*	200 nm – 990 nm	0.3 nm
HR4000 from *OceanOptics*	700 nm – 1.1 μm	0.2 nm
NIR512 from *OceanOptics*	850 nm – 1.6 μm	1 nm
NaCl prism monochromator with a PbSe detector	1 μm – 5 μm	0.3 μm
NaCl prism monochromator with a HgCdTe detector	2 μm – 14 μm	0.2 μm

This page intentionally left blank.

4 Results

Figure 12a presents the angularly resolved supercontinuum distribution from filaments generated in air with laser pulses having a peak power of 1.4 TW (pulse duration of 42 fs, energy of 60 mJ). The peak power was 140 times higher than the critical power (Pcr=10 GW) for self-focusing in air [24], and thus, multiple filaments were generated. Because of the highly nonlinear processes involved in the supercontinuum generation, it was not possible to clearly detect the FIR signal at lower pulse powers. Also, because of the high peak power used, any small hot spots in the initial laser beam profile induced their own filaments, and thus their own CE. The multiple CEs generated at different zones in the filaments limited the angular resolution of the spectrum. However, we can distinguish in Figure 12a the referenced CE in the UV from both the supercontinuum and the generated third harmonic (TH) in air [25, 26].

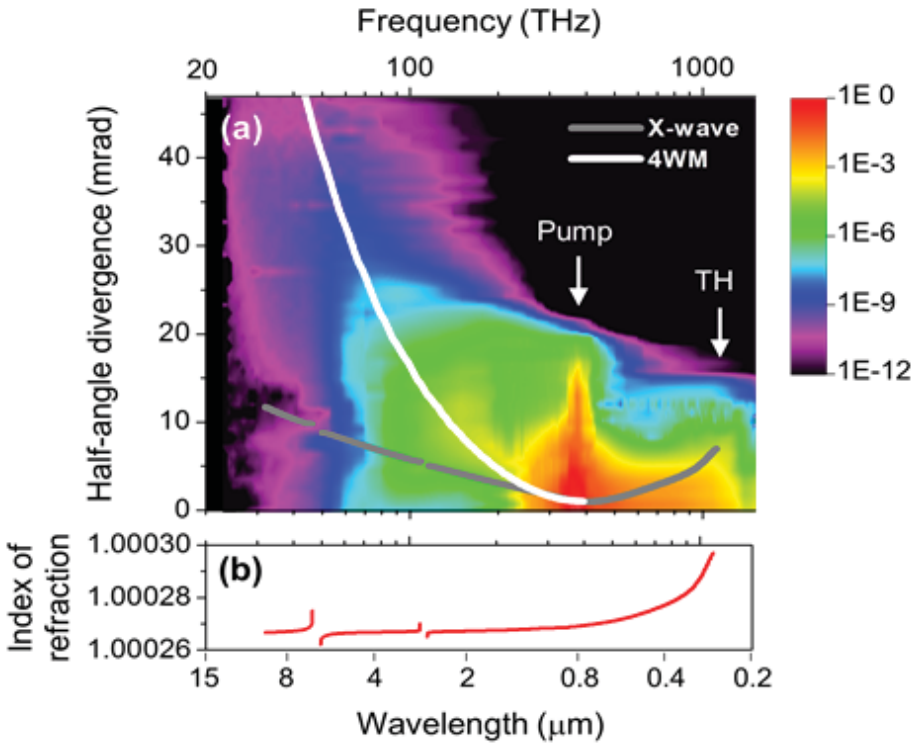

Figure 12. *(a) Angularly resolved spectrum generated during the filamentation in air by ultrashort and intense laser pulses. The horizontal axis is a logarithmic scale for the frequency. The false colors associated with the spectrum are related to the relative spectral intensity. The white arrows point out the central frequency of the pump pulse and its third harmonic (TH).*
(b) The linear refractive index of air calculated using a Sellmeier-type model.

Interpretation of Figure 12 is complex and needs analysis based on new theory for the nonlinear propagation of powerful laser pulses. Recently accepted by the majority of the scientific community in the area, the theory (named X-waves theory) considered the dispersion and the

group velocity of the laser pulse in order to explain the CE generated during the filamention. With this more complete theory, the divergence of the visible and UV conical emission can be fitted with the X-wave dispersion relation (grey line on Figure 12a) given by $\theta(\omega) = tan^{-1}\left(\sqrt{k^2 - k_z^2}/k_z\right)$, where θ is the half-angle divergence of the CE, $k = \omega n(\omega)/c$ is the wavevector at the angular frequency ω, $k_z = (k_0 - \beta) + (k_0' - \gamma)(\omega - \omega_0)$ is the longitudinal component of the wavevector, k_0' is the first derivative of $k(\omega)$ evaluated at the central frequency ω_0, γ and β are correction factors for the phase and group velocity, respectively [27]. It is interesting to note that the angularly resolved spectrum presents a broad IR CE beginning at 1.4 μm up to 13.6 μm. However, the new X-wave dispersion relation (grey line in Figure 12a) calculated according to the linear refractive index of air [28] given in Figure 12b did not fit the IR CE observed at large divergence angles. Different values of γ and β have been tested in order to fit the experimental results. However, no qualitative agreements have been found for both the visible CE and these IR radiations diverging at large angles.

Therefore, it means that another mechanism for the generation of the IR CE must be considered, and it is the first time in the scientific literature that such infrared extension of the white-light supercontinuum has been observed. The most probable process to explain the observed IR CE is the parametric generation through the 4WM between the pump frequency (ω_0) and its blue-shifted conical emission (ω_{CE}). The 4WM frequency is given by $\omega_{4WM} = 2\omega_0 - \omega_{CE}$, the wavevector $\vec{k}_{4WM} = 2\vec{k}_0 - \vec{k}_{CE}$ and the half-angle divergence (white line in Figure 12a) corresponds to

$$\theta_{4WM}(\omega) = tan^{-1}(k_r/(2k_0 - k_z)) = tan^{-1}\left(\sqrt{k^2 - k_z^2}/(2k_0 - k_z)\right) \quad (13)$$

where k_z and k_r are the longitudinal and the radial components of the blue-shifted CE wavevector, respectively. The calculations were done assuming a collimated pump pulse in the filament zone and the divergence of the blue-shifted CE was estimated according to the X-wave dispersion relation by assuming γ and β equal to zero. Using this simple equation, we quantitatively fit (white line in Figure 12a) the strong IR CE observed in the angularly resolved spectrum. Even though the 4WM mechanism was not perfectly phase-matched over the complete spectral range (coherence length $\pi/\Delta k$ is at least 5 mm long for all IR wavelengths), the divergence of the blue-shifted CE limited the co-propagation distance with its pump inside the filament zone. In fact, by assuming a filament diameter of 70 μm [29] and the divergence of the blue-shifted CE, the pump pulse and the CE co-propagated on a distance shorter than their coherence length when the CE diffracts/refracts out of the filament; which guaranteed a constructive 4WM generation.

Figure 13 shows the measured and the calculated spatial profiles of the IR signal at 2 μm, 4 μm and 8 μm. The calculations are done by mixing each spectral component of the pump at the end of the filament (i.e., $\Delta\lambda_{FWHM}$=80 nm) with the blue-shifted CE. The experimental width of the IR CE is slightly larger than the calculation due to the multiple filaments generated by the pump pulses. From Figure 12a and Figure 13, we observed that the infrared contribution to the supercontinuum for wavelengths longer than 1.4 μm is mainly due to the 4WM between the pump pulse and its blue-shifted CE. There is only an IR central spot appearing between 4 μm and 9.4 μm, which cannot be explained by the off-axis 4WM process. It is possible that the on-axis IR

radiation originated from the Kerr self-phase modulation or an on-axis 4WM process originating from a self-phase locking mechanism [4, 30]. It is important to note that, the thermal emission from the plasma generated during the filamentation, did not contribute to the angularly resolved spectrum measured in Figure 12a. This observation was verified by positioning the spectrometers perpendicularly at 10 cm to the bunch of filaments. No fluorescence or thermal emission was detected in the IR range.

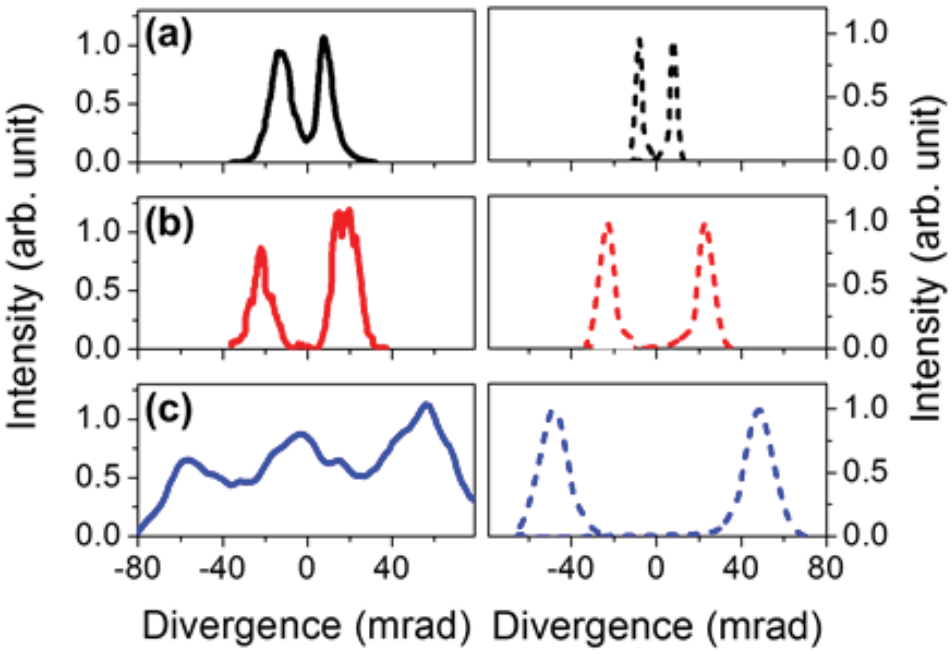

Figure 13. *Spatial distribution of the infrared conical emission measured (left column) and calculated (right column) at (a) 2 μm, (b) 4 μm, and (c) 8 μm.*

Figure 14 presents the spatially integrated supercontinuum generated in air by fs-TW laser pulses, where the horizontal axis is a linear scale expressed in units of wavelength. Figure 14 clearly shows the long IR extension of the supercontinuum that completely covered the optical transmission windows of the atmosphere. There are also dips in the IR extension, which correspond to the absorption bands of water vapour and carbon dioxide in air [31]. These dips in the supercontinuum are not very pronounced because the propagation distance between the filaments and the spectrometers was only 3 m long and the limited resolution of the spectrometers blurred these absorption bands. The cut-off at the ultraviolet extension of the supercontinuum is due to the strong O_2 absorption for wavelength below 200 nm.

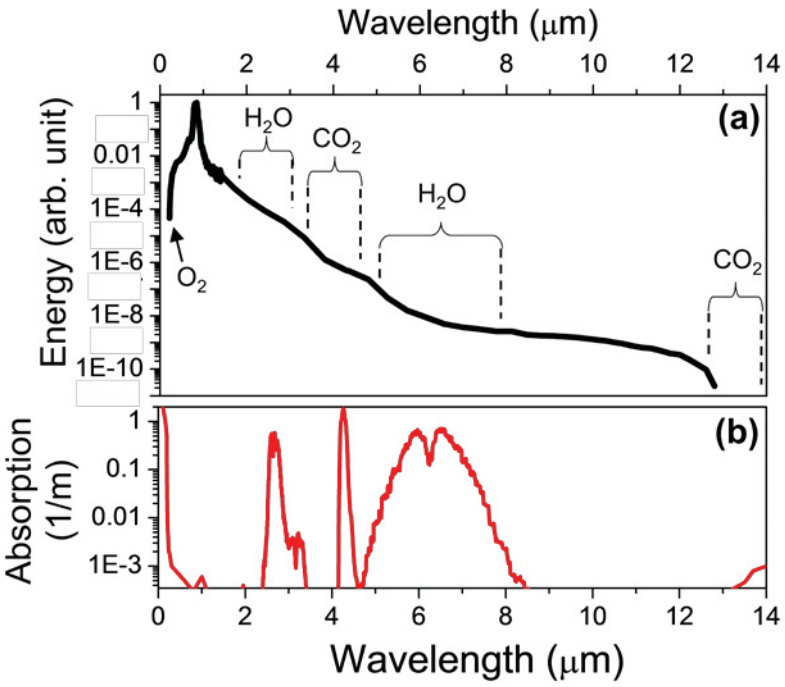

Figure 14. *(a) Spatially integrated supercontinuum generated during the filamentation in air of an ultrashort and intense laser pulse. (b) Absorption spectrum of air for a pressure of 1 atmosphere, a temperature of 15 ºC, and a relative humidity of 40%.*

5 Conclusion

In conclusion, we obtained the complete optical spectrum generated during the filamentation of fs-TW pulses in air. The angularly resolved supercontinuum spanned from 200 nm up to 13.6 μm. Surprisingly, the radiation generated in the MIR and FIR regions was mainly attributed to the 4WM between the pump pulse and its blue-shifted CE, and not to the spectral broadening from the self-phase modulation. The spectral extension of the fs-TW laser propagating in the air was so broad that the generated white-light laser burst could overpass the absorption of air and produce remote IR sources in the 3-5 μm and 8-12 μm regions. The peak intensity of the generated IR pulse inside each optical filament was around 50 MW/cm^2 and 50 kW/cm^2 in the MIR and FIR spectral regions, respectively. These results may suggest that the spectral intensity of the IR supercontinuum could even be strongly enhanced by mixing two delayed pump pulses or by mixing a pump pulse with another laser pulse in the visible range. Such broadband white-light laser would have interesting applications for the IR remote sensing of pollutants or for CM applications based on dazzling optical devices.

The future analysis that must be done is the characterization of the white-light laser at longer propagation distance in the atmosphere. Because there are numerous physical processes interacting during the filamentation, the evolution of the white-light laser pulse is probably different at long distance in the atmosphere, due to some physical processes like the dispersion and the diffraction becoming more important at long distances –these phenomena might affect the dynamic equilibrium of the filamentation and result in a narrower or broader white-light burst.

Finally, it should be noted that the fs laser technology has evolved very quickly during the last few years. Recently, a direct diode-pumped fs laser medium, namely Ytterbium doped Potassium Gadolinium Tungstate [32], has been discovered and has proven to be an efficient gain medium for building a compact and robust fs sources. The 500 fs pulse duration, and central wavelength of 1 μm, might also enhance the efficiency of generating a white-light laser pulse, because recent simulations [33] have shown that a filamentating laser pulse having an initial central wavelength around 1 μm generates a broader white-light laser pulse than an 800 nm laser pulse.

This page intentionally left blank.

References

[1] W. Liu, S. A. Hosseini, Q. Luo, B. Ferland, S. L. Chin, O. G. Kosareva, N. A. Panov and V. P. Kandidov, "Experimental observation and simulations of the self-action of white light laser pulse propagating in air, " New Journal of Physics, **6**, 6 (2004).

[2] B. Prade, M. Franco, A. Mysyrowicz, A. Couairon, H. Buersing, B. Eberle, M. Krenz, D. Seiffer, and O. Vasseur, "Spatial mode cleaning by femtosecond filamentation in air," Opt. Lett. **31**, 2601 (2006)..

[3] F. Théberge, N. Aközbek, W. Liu, A. Becker, and S.L. Chin, "Tunable Ultrashort Laser Pulses Generated through Filamentation in Gases," Phys. Rev. Lett. **97**, 023904 (2006).

[4] S.L. Chin, F. Théberge, and W. Liu, "Filamentation nonlinear optics," Appl. Phys. B: Lasers Opt. **86**, 477 (2007).

[5] M. Châteauneuf, J. Dubois, and F. Théberge, "Microwave guided in a laser plasma induced waveguide," Technical Report, DRDC-Valcartier (submitted December 2009).

[6] M. Rodriguez, R. Sauerbrey, H. Wille, L. Wöste, T. Fujii, Y.-B. André, A. Mysyrowicz, L. Klingbeil, K. Rethmeier, W. Kalkner, J. Kasparian, E. Salmon, J. Yu, and J.-P. Wolf, "Triggering and guiding megavolt discharges by use of laser-induced ionized filaments," Opt. Lett. **27**, 772 (2002).

[7] M. Hercher, "Laser-induced damage in transparent media," J. Opt. Soc. Am. **54**, 563 (1964).

[8] Y.R. Shen, "Self-Focusing: Experimental," Prog. Quant. Electr. **4**, 1 (1975).

[9] J.H. Marburger, "Self-focusing theory," Prog. Quant. Electr. **4**, 35 (1975).

[10] D. Strickland, and G. Mourou, "Compression of amplified chirped optical pulses," Opt. Comm. **56**, 219 (1985).

[11] P. Maine, D. Strick, P. Bado, M. Pessot, and G. Mourou, "Generation of ultrahigh peak power pulses by chirped pulse amplification," IEEE J. of Quant. Electron. 24, 298 (1988).

[12] S.L. Chin, S.A. Hosseini, W. Liu, Q. Luo, F. Théberge, N. Ak?zbek, A. Becker, V.P. Kandidov, O.G. Kosareva, and H. Schroeder, "The propagation of powerful femtosecond laser pulses in optical media: physics, applications, and new challenges," Canadian Journal of Physics, **83**, 863 (2005)

[13] A. Couairon, and A. Mysyrowicz, "Femtosecond filamentation in transparent media," Phys. Rep. **441**, 47 (2007).

[14] H.R. Lange, A. Chiron, J.-F. Ripoche, A. Mysyrowicz, P. Breger, and P. Agostini, "High-Order Harmonic Generation and Quasiphase Matching in Xenon Using Self-Guided Femtosecond Pulses," Phys. Rev. Lett. **81**, 1611 (1998).

[15] J. Kasparian, R. Sauerbrey, and S. L. Chin, "The critical laser intensity of self-guided light filaments in air," Appl. Phys. B: Lasers Opt. **71**, 877 (2000).

[16] W. Liu, F. Theberge, J.-F. Daigle, P.T. Simard, S.M. Sarifi, Y. Kamali, H.L. Xu, and S.L. Chin, "An efficient control of ultrashort laser filament location in air for the purpose of remote sensing," Applied Physics B, **85**, 55 (2006).

[17] A Brodeur, C Y Chien, F A Ilkov, S L Chin, O G Kosareva, and V P Kandidov, "Moving focus in the propagation of powerful ultrashort laser pulses in air," Optics Letters, **22**, 304 (1997)

[18] M. Mlejnek, E. M. Wright, and J. V. Moloney, "Dynamic spatial replenishment of femtosecond pulses propagating in air," Opt. Lett., **23**, 382 (1998).

[19] S.L. Chin, H.L. Xu, Q. Luo, F. Théberge, W. Liu, J.F. Daigle, Y. Kamali, P.T. Simard, J. Bernhardt, S.A. Hosseini, M. Sharifi, G. Méjean, A. Azarm, C. Marceau, O. Kosareva, V.P. Kandidov, N. Aközbek, A. Becker, G. Roy, P. Mathieu, J.R. Simard, M. Châteauneuf, and J. Dubois, "Filamentation "remote" sensing of chemical and biological agents/pollutants using only one femtosecond laser source," Appl. Phys. B, **95**, 1 (2009).

[20] J. Kasparian, R. Ackermann, Y.-B. André, G. Méchain, G. Méjean, B. Prade, P. Rohwetter, E. Salmon, K.Stelmaszczyk, J. Yu, A. Mysyrowicz, R. Sauerbrey, L.Wöste, and J.-P. Wolf, "Electric events synchronized with laser filaments in thunderclouds," Opt. Express **16**, 5757 (2008).

[21] M. Châteauneuf, S. Payeur, J. Dubois, and J.-C. Kieffer, "Microwave guiding in air by a cylindrical filament array waveguide," Appl. Phys. Lett. **92**, 091104 (2008).

[22] F. Théberge, W. Liu, Q. Luo, and S. L. Chin, "Ultrabroadband continuum generated in air (down to 230 nm) using ultrashort and intense laser pulses," Applied Physics B, **80**, 221 - 225 (2005).

[23] J. Kasparian, R. Sauerbrey, D. Mondelain, S. Niedermeier, J. Yu, J.-P. Wolf, Y.-B. André, M. Franco, B. Prade, S. Tzortzakis, A. Mysyrowicz, M. Rodriguez, H. Wille, and L. Wöste, "Infrared extension of the supercontinuum generated by femtosecond terawatt laser pulses propagating in the atmosphere," Opt. Lett. **25**, 1397 (2000).

[24] W. Liu and S. L. Chin, "Direct measurement of the critical power of femtosecond Ti:sapphire laser pulse in air," Optics Express, **13**, 5750 (2005).

[25] M. Kolesik, E. M. Wright, and J. V. Moloney, "Supercontinuum and third-harmonic generation accompanying optical filamentation as first-order scattering processes," Opt. Lett. **32**, 2816 (2007).

[26] M. Kolesik, E. M. Wright, A. Becker, and J. V. Moloney, "Simulation of third-harmonic and supercontinuum generation for femtosecond pulses in air," Appl. Phys. B **85**, 531 (2006).

[27] D. Faccio, A. Averchi, A. Couairon, M. Kolesik, J. V. Moloney, A. Dubietis, G. Tamosauskas, P. Polesana, A. Piskarskas, and P. Di Trapani, "Spatio-temporal reshaping and X-Wave dynamics in optical filaments," Opt. Express **15**, 13077 (2007).

[28] M. E. Thomas and D. D. Duncan, "The Infrared & ElectroOptical Systems Handbook," Vol. 2 of *Atmospheric Propagation of Radiation*, F. Smith, ed., SPIE, Chap. 1, 88 (1993).

[29] F. Théberge, W. Liu, P. Tr. Simard, A. Becker, and S. L. Chin, "Plasma density inside a femtosecond laser filament in air: Strong dependence on external focusing," Physical Review E, **74**, 036406 (2006).

[30] N. Aközbek, A. Iwasaki, A. Becker, M. Scalora, S. L. Chin, and C. M. Bowden, "Third-Harmonic Generation and Self-Channeling in Air Using High-Power Femtosecond Laser Pulses," Phys. Rev. Lett., **89**, 143901 (2002).

[31] P. K. Acharya, A. Berk, G. P. Anderson, N. F. Larsen, S.-C. Tsay, and K. H. Stamnes, "MODTRAN4: multiple scattering and bidirectional reflectance distribution function (BRDF) upgrades to MODTRAN," Proc. SPIE **3756**, 354 (1999).

[32] A. Krueger, and P. Féru, "Ytterbium Tungstate Revolutionizes the Field of High-Power Ultrafast Lasers," Photonics Spectra, March issue, (2004).

[33] N. Aközbek, A. Becker, M. Scalora, S.L. Chin, C.M. Bowden, "Continuum generation of the third-harmonic pulse generated by an intense femtosecond IR laser pulse in air," Applied Physics B, **77**, 177-183 (2003).

This page intentionally left blank.

List of symbols/abbreviations/acronyms/initialisms

a	radius of laser beam at 1/e of intensity
c	speed of light
CE	Conical Emission
CM	Counter-Measure
CPA	Chirped Pulse Amplification
d	grating groove period
DND	Department of National Defence
DRDC	Defence Research & Development Canada
DRDKIM	Director Research and Development Knowledge and Information Management
e	charge of electron
FIR	Far-infrared
fs	femtosecond
FWHM	Full Width at Half Maximum
GW	Gigawatt
I	laser intensity
IR	Infrared
k	wavevector
k_r	radial component of the wavevector
k_z	longitudinal component of the wavevector
m	diffraction order
MCT	Mercury-Cadmium-Tellurium
m_e	mass of electron
MW	Megawatt
MIR	Mid-infrared
N_e	plasma density
n_0	linear index of refraction
n_2	nonlinear index of refraction
P	peak power of the laser pulse
P_{cr}	Critical power for self-focusing

r	radial coordinate
R&D	Research & Development
SPM	Self-Phase Modulation
t	temporal coordinate
T&T Lab	Terawatt & Terahertz Laboratory
TH	Third Harmonic
TW	Terawatt
UV	Ultraviolet
w	effective ionization rate
z_f	self-focusing distance
β	correction factor for the group velocity (X-wave theory)
γ	correction factor for the phase velocity (X-wave theory)
λ	wavelength
θ	angle of the beam to the normal of the surface
τ	period of a optical cycle
ω_p	plasma frequency
ω_0	central frequency of the laser
4WM	four-wave mixing

DOCUMENT CONTROL DATA

(Security markings for the title, abstract and indexing annotation must be entered when the document is Classified or Designated)

1. ORIGINATOR (The name and address of the organization preparing the document. Organizations for whom the document was prepared, e.g. Centre sponsoring a contractor's report, or tasking agency, are entered in section 8.)

Defence Research and Development Canada – Valcartier
2459 Pie-XI Blvd North
Quebec (Quebec)
G3J 1X5 Canada

2a. SECURITY MARKING (Overall security marking of the document including special supplemental markings if applicable.)

UNCLASSIFIED

2b. CONTROLLED GOODS

(NON-CONTROLLED GOODS)
DMC A
REVIEW: GCEC JUNE 2010

3. TITLE (The complete document title as indicated on the title page. Its classification should be indicated by the appropriate abbreviation (S, C or U) in parentheses after the title.)

White-light burst generated during the filamentation of a Terawatt laser beam

4. AUTHORS (last name, followed by initials – ranks, titles, etc. not to be used)

Théberge, F., Châteauneuf, M., J. Dubois, J., Mathieu, P.

5. DATE OF PUBLICATION (Month and year of publication of document.)	6a. NO. OF PAGES (Total containing information, including Annexes, Appendices, etc.)	6b. NO. OF REFS (Total cited in document.)
June 2011	44	33

7. DESCRIPTIVE NOTES (The category of the document, e.g. technical report, technical note or memorandum. If appropriate, enter the type of report, e.g. interim, progress, summary, annual or final. Give the inclusive dates when a specific reporting period is covered.)

Technical Report

8. SPONSORING ACTIVITY (The name of the department project office or laboratory sponsoring the research and development – include address.)

Defence Research and Development Canada – Valcartier
2459 Pie-XI Blvd North
Quebec (Quebec)
G3J 1X5 Canada

9a. PROJECT OR GRANT NO. (If appropriate, the applicable research and development project or grant number under which the document was written. Please specify whether project or grant.)	9b. CONTRACT NO. (If appropriate, the applicable number under which the document was written.)
13NH01	

10a. ORIGINATOR'S DOCUMENT NUMBER (The official document number by which the document is identified by the originating activity. This number must be unique to this document.)	10b. OTHER DOCUMENT NO(s). (Any other numbers which may be assigned this document either by the originator or by the sponsor.)
DRDC Valcartier TR 2010-416	

11. DOCUMENT AVAILABILITY (Any limitations on further dissemination of the document, other than those imposed by security classification.)

Unlimited

12. DOCUMENT ANNOUNCEMENT (Any limitation to the bibliographic announcement of this document. This will normally correspond to the Document Availability (11). However, where further distribution (beyond the audience specified in (11) is possible, a wider announcement audience may be selected.))

Unlimited

13. ABSTRACT (A brief and factual summary of the document. It may also appear elsewhere in the body of the document itself. It is highly desirable that the abstract of classified documents be unclassified. Each paragraph of the abstract shall begin with an indication of the security classification of the information in the paragraph (unless the document itself is unclassified) represented as (S), (C), (R), or (U). It is not necessary to include here abstracts in both official languages unless the text is bilingual.)

Defence Research & Development Canada—Valcartier (DRDC Valcartier) initiated many projects on femtosecond laser based counter-measure applications. One of the main properties of high peak power femtosecond laser pulses is their transformation into a white-light supercontinuum, which can be exploited for dazzle (and possibly damage) counter-measure purposes. Contrary to normal dazzle generated using a narrow-spectrum laser source, the white-light surpercontinuum from femtosecond laser pulses spans continuously from the ultraviolet up to the infrared. Such broadband white-light lasers are virtually impossible to block because they do not rely on a single wavelength to achieve the effect. This report presents the characterization of the white-light laser burst produced during the propagation in air of a femtosecond-Terawatt laser. The supercontinuum was generated from 200 nm in the ultraviolet up to 13.6 μm in the far infrared, which led to the first worldwide demonstration of such a broadband laser source.

Recherche et développement pour la défense Canada—Valcartier (RDDC Valcartier) a entrepris plusieurs projets sur les sources lasers femtosecondes pour des applications de contre-mesures. L'une des principales propriétés des impulsions laser femtoseconde de haute puissance est leur transformation en une impulsion de lumière blanche qui pourrait être utilisée comme contre-mesure pour éblouir (et possiblement endommager) les détecteurs optiques. Contrairement aux contre-mesures laser basées sur des sources à spectres étroits, l'impulsion de lumière blanche générée par le laser femtoseconde comporte un spectre très large pouvant s'étendre de l'ultraviolet jusqu'à l'infrarouge. Un tel laser blanc est virtuellement impossible à contrer, car il n'est pas basé sur une seule longueur d'onde pour générer l'effet désiré. Ce rapport présente la caractérisation de l'impulsion laser blanche produite durant la propagation d'un laser femtoseconde-térawatt dans l'air. Le supercontinuum du laser blanc s'étend de 200 nm dans l'ultraviolet jusqu'à 13,6 μm dans l'infrarouge lointain, ce qui correspond à la première démonstration mondiale d'une telle source laser à très large spectre.

14. KEYWORDS, DESCRIPTORS or IDENTIFIERS (Technically meaningful terms or short phrases that characterize a document and could be helpful in cataloguing the document. They should be selected so that no security classification is required. Identifiers, such as equipment model designation, trade name, military project code name, geographic location may also be included. If possible keywords should be selected from a published thesaurus, e.g. Thesaurus of Engineering and Scientific Terms (TEST) and that thesaurus identified. If it is not possible to select indexing terms which are Unclassified, the classification of each should be indicated as with the title.)

femtosecond-terawatt; filament; white-light laser; counter-measure

Defence R&D Canada

Canada's Leader in Defence
and National Security
Science and Technology

R & D pour la défense Canada

Chef de file au Canada en matière
de science et de technologie pour
la défense et la sécurité nationale

www.drdc-rddc.gc.ca